ACS OMEGA

http://pubs.acs.org/journal/acsodf

Article

Aerosol-Printed MoS_2 Ink as a High Sensitivity Humidity Sensor

Neuma M. Pereira, Natália P. Rezende, Thiago H. R. Cunha, Ana P. M. Barboza, Glaura G. Silva, Daniel Lippross, Bernardo R. A. Neves, Hélio Chacham, Andre S. Ferlauto, and Rodrigo G. Lacerda*

Cite This: *ACS Omega* 2022, 7, 9388−9396

Read Online

ACCESS | Metrics & More | Article Recommendations | Supporting Information

ABSTRACT: Molybdenum disulfide (MoS_2) is attractive for use in next-generation nanoelectronic devices and exhibits great potential for humidity sensing applications. Herein, MoS_2 ink was successfully prepared via a simple exfoliation method by sonication. The structural and surface morphology of a deposited ink film was analyzed by scanning electron microscopy (SEM), Raman spectroscopy, and atomic force microscopy (AFM). The aerosol-printed MoS_2 ink sensor has high sensitivity, with a conductivity increase by 6 orders of magnitude upon relative humidity increase from 10 to 95% at room temperature. The sensor also has fast response/recovery times and excellent repeatability. Possible mechanisms for the water-induced conductivity increase are discussed. An analytical model that encompasses two ionic conduction regimes, with a percolation transition to an insulating state below a low humidity threshold, describes the sensor response successfully. In conclusion, our work provides a low-cost and straightforward strategy for fabricating a high-performance humidity sensor and fundamental insights into the sensing mechanism.

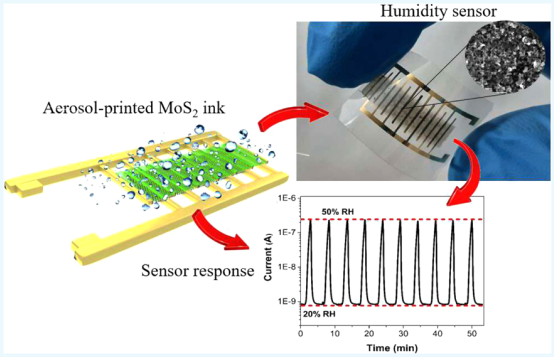

INTRODUCTION

In recent years, printing technologies have increasingly been used to replace conventional semiconductor device technologies for the fabrication of ultra-low-cost electronic components.[1] Inks containing different classes of materials can be used to print functional components such as semiconducting layers, resistors, and dielectrics[2] over different types of (flexible) substrates.[3] In this context, a blooming field is the development of sensors that cover a wide area of applications such as real-time biomonitoring, wearables, environmental monitoring, industrial process control, and personal safety.[4−6] In particular, an area of interest is humidity sensors, which have had an increasing demand for use in environmental control and industrial processing.[7] For instance, humidity is closely monitored in the semiconductor industry, as devices and integrated circuits, printed circuit boards, electronic components, and data are highly sensitive to humidity.[8] Similarly, several industrial processes such as chemical purification of gases, using dryers and ovens, paper production and textiles, and food processing, require high control of humidity.[7] Thus, it is highly desirable to develop low-cost humidity sensors integrated into different surfaces and portable devices.[9,10] Several materials have been studied for their humidity sensing capabilities, such as polymers,[11,12] metal oxides,[13,14] carbon nanomaterials,[9,15,16] cellulose,[17,18] and transition metal dichalcogenides (TMDs).[19−23] Two-dimensional (2D) transition metal dichalcogenides, such as molybdenum disulfide (MoS_2), are becoming significant materials in various research fields and, specially, for sensing applications. Recently, MoS_2 has received increasing attention in ultrasensitive sensor applications to detect different gases, such as NO_2, NH_3, H_2, and water molecules.[21,24−26]

Conductive ink formulations are still far from ideal, as they require substrate functionalization[27] or lengthy and expensive formulation processing.[28,29] They are also usually based on toxic and expensive solvents and additives or need relatively high temperatures to dry,[30] restricting their application to specific substrates. Alternatively, the use of aqueous dispersions as inks for printing on multiple devices can be an approach to replace nonsustainable and expensive methods.[31,32] However, the development of new inks composed of functional materials, with different readily available properties, that are both sustainable and inexpensive still is in its infancy.[33] Recently, several works in the literature have shown the development of water-based inks of 2D materials.[23,34] For instance, Casiraghi et al.[23] developed water-based and biocompatible graphene and hBN inks to fabricate all-2D material and inkjet-printed capacitors. In another work, McManus et al.[35] developed photodetectors inkjet-printed on paper using graphene as electrodes and TMDs such as MoS_2, WS_2, $MoSe_2$, and $MoTe_2$ as photoactive components.[34,36] Among various types of TMD

Received: November 19, 2021
Accepted: March 1, 2022
Published: March 10, 2022

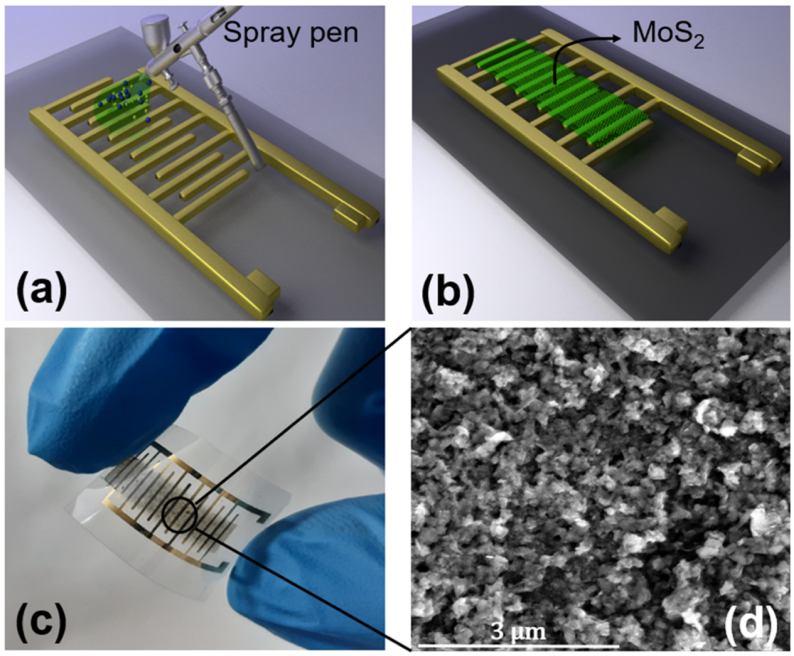

Figure 1. (a) Schematic representation of the humidity sensor preparation: a spray pen was employed to apply a uniformly MoS_2 ink layer on a PET substrate with previously Au-deposited interdigitated electrodes and (b) humidity sensor with the MoS_2 sensing material deposited. (c) Picture of the MoS_2 film sensor on a flexible PET substrate. (d) SEM micrograph of the surface morphology of the MoS_2 film.

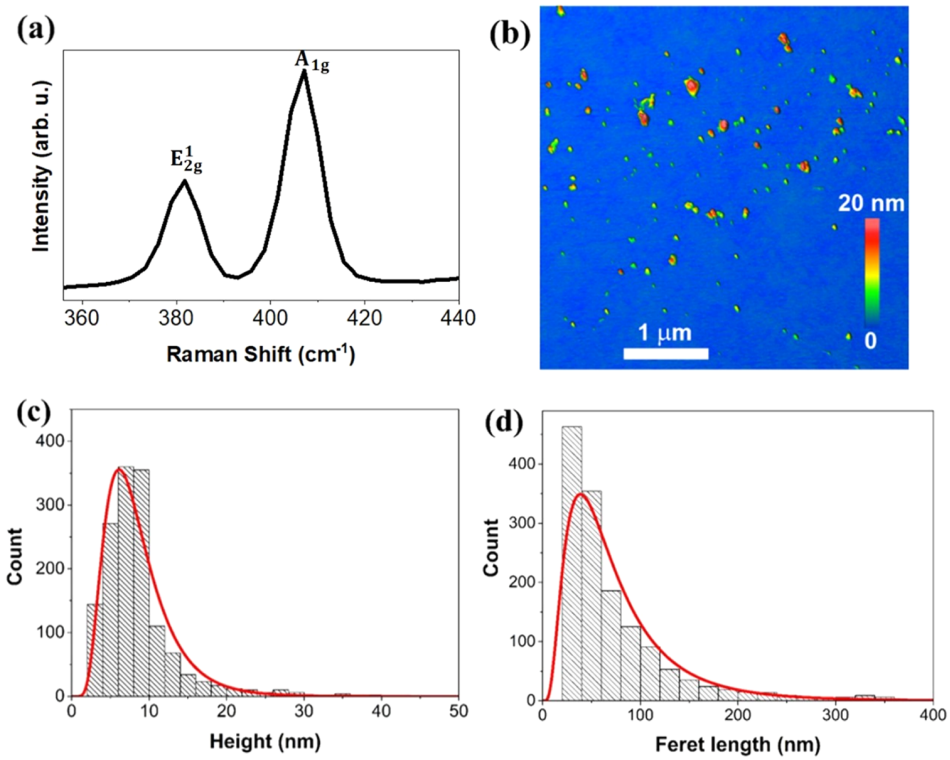

Figure 2. (a) Raman spectrum of the MoS_2 film. The separation between the position of the $E_{2g}{}^1$ and A_{1g} peaks (25.7 cm^{-1}) indicates that the flakes have multiple layers (>7 layers). (b) AFM image of MoS_2 flakes. (c) Histogram of the average height distribution of the MoS_2 flakes. (d) Distribution of Feret length of MoS_2 flakes. A lognormal distribution (solid line) was fitted to the data to determine the mode of the MoS_2 height and length distributions.

preparation, liquid-phase exfoliation (LPE) by sonication is considered a low-cost, simple, and versatile method with high potential for scale-up.[37] This work presents a low-cost, stable, and printable MoS_2 ink for high-performance humidity sensors. No harsh conditions, solvent exchange, or chemical treatments were used, which allow the application to several substrates, including flexible substrates. The aerosol-printed MoS_2 sensor exhibit high sensitivity (10^5–10^6%) with response/recovery

https://doi.org/10.1021/acsomega.1c06525
ACS Omega 2022, 7, 9388−9396

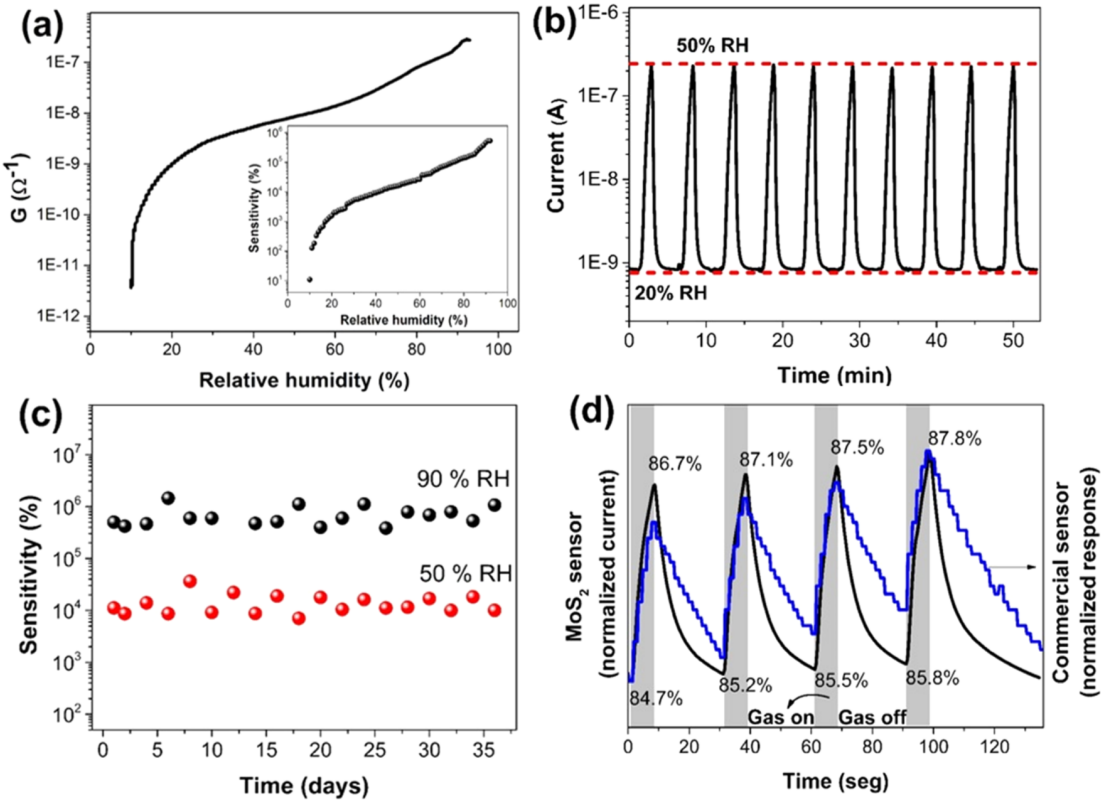

Figure 3. (a) Conductance values of a MoS_2 sensor in a copper-clad phenolic sheet, determined from the fixed applied voltage of 10 V, as a function of the relative humidity (RH). Inset: Device sensitivity S (see eq 1) versus RH. (b) Repeatability performance of the MoS_2 sensor exposed to cyclic variations of RH between 20 and 50%. (c) Stability of the MoS_2 humidity sensor at 50 and 95% RH during a period of 40 days. (d) Response and recovery dynamics of the MoS_2 (black) and commercial (blue) sensors to sudden changes in relative humidity.

times comparable to commercial humidity sensors and excellent repeatability. Possible mechanisms for the water-induced conductivity increase are discussed, and an analytical model that encompasses two conduction regimes, depending on relative humidity (RH), is proposed and describes the sensor response to RH successfully. We believe that our device can significantly influence the application of MoS_2 ink for humidity sensors.

RESULTS AND DISCUSSION

Material Characterization. Figure 1 shows a schematic illustration of the sensor preparation, described in detail in the Experimental Section (Figure 1a,b), with a representative picture of the device of the MoS_2 film sensor on a flexible PET substrate (Figure 1c) and typical scanning electron microscopy (SEM) micrograph of the surface morphology of the film (Figure 1d). Details of the MoS_2 ink sensor deposited on flexible (PET) substrate response to humidity are shown in the Support Information.

The SEM image presented in the inset of Figure 1d reveals that the deposited MoS_2 sensing film is continuous and composed of an interconnected array of MoS_2 flakes that densely cover the entire device area forming a 3D-like nanostructure film. A large number (~50) of spray scans were performed to ensure film continuity in the active region. Raman spectroscopy was employed to investigate the structural properties of the as-deposited MoS_2 films (Figure 2a). Two active Raman active modes, E_{2g}^1 at 381.1 cm^{-1} and A_{1g} at 406.8 cm^{-1}, associated with the hexagonal MoS_2 structure, are observed as expected. The A_{1g} mode is associated with the out-of-plane vibration of S atoms only in opposite directions, whereas E_{2g}^1 results from the opposite vibration of two S atoms with respect to the Mo atom.[39−41] The frequency difference between the A_{1g} and E_{2g}^1 Raman modes can be correlated to the number of MoS_2 layers in the crystal. The obtained value of 25.7 cm^{-1} indicates that MoS_2 flakes have multiple layers (>7 layers).[42]

To perform the AFM measurements, the MoS_2 ink was deposited on a Si wafer by drop-casting. To provide a representative statistical analysis of the material, nine images over distinct regions of the sample were acquired with a lateral size of 5 μm with 500 × 500 pixels. The lateral size of the MoS_2 flakes was defined as the maximum Feret length and the height as the mean height value of the flakes.[43] This analysis followed the methodology developed by Fernandes et al.,[43] which provided a semiautomated statistical analysis of the thickness and size of graphene systems.

A representative AFM image of the MoS_2 nanoflakes is shown in Figure 2b. The corresponding height and Feret length distributions are shown in Figure 2c,d, respectively. The modal height of the MoS_2 flakes was 6.2 ± 5.7 nm (Figure 2c), which corresponds to around 10 layers, which is consistent with the number of layers estimated by Raman analysis (separation between the position of the E_{2g}^1 and A_{1g} peaks (25.7 cm^{-1})), which indicates that the number of layers would be higher than 7 nm.[42] The modal Feret length obtained was 28.2 ± 104.1 nm (Figure 2d). The characteristic length/thickness aspect ratio, obtained from the modal values discussed above, is 4.5. Such value of ratio can be considered

https://doi.org/10.1021/acsomega.1c06525
ACS Omega 2022, 7, 9388−9396

Table 1. Properties Comparison of the MoS_2 Humidity Sensor and Reported Humidity Sensors

sensing material	sensor type	detection range (RH) (%)	sensitivity (%)	response time (s)	recovery time (s)	reference
MoS_2	FET	0−35	10^4	10	60	49
MWCNT/Nafion nanofibers film	surface acoustic wave resonator	10−80	427.6	3	63	50
MoS2 QDs synthesized in NMP	impedance	10−95	2.27×10^6	14	280	44
graphene/ZnO	impedance	0−85	NA	1	2	51
glycidyl trimethyl ammonium chloride/cellulose	impedance	11−95	>67.3	25	188	52
2D hBN-poly(ethylene oxide)	impedance	0−90	2160	2.6	2.8	53
dendritic MoS_2	impedance	11−95	3031	11	17	21
2D MoS_2-PEDOT:PSS	impedance	0−80	4000	0.5	0.8	54
PEDOT:PSS/GO	impedance	0−100	2.6×10^4	1	3.5	55
halloysite nanotubes	impedance	0−91.5	10^5	0.7	57.5	56
TiO_2/(K,Na)NbO_3	impedance	12−94	1.6×10^5	25	38	57
BEHP-co-MEH: PPV-PAA.PSS	capacitive	0−80	NA	3.5	5	58
poly(dimethylsiloxane)/$CaCl_2$	capacitive	30−95	10.2	120		59
GO	capacitive	30−90	209	∼200	∼100	9
ITO/alumina	capacitive	5−95	737.2	47.2	49.5	60
MoS_2/nanodiamond	capacitive	11−97	∼3500	<1	0.9	61
carbon dots	capacitive	20−90	6300			62
GO/MWCNT	capacitive	11−97	7980	5	2.5	63
poly(ethylene oxide)/CuO/MWCNT	capacitive	30−90	53837.6	20	11	64
MoS_2/SnO_2	capacitive	0−97	3.3×10^6	5	13	65
MWCNT/HEC	resistive	20−80	3.84	∼20	∼35	66
SnO_2/rGO	resistive	11−97	45.02	∼90	∼100	67
PEDOT:rGO-PEI/Au NPs	resistive	11−98	51.6	20	35	68
printed MWCNTs	resistive	30−60	57.6			69
MoS_2/PVP	resistive	11−94	80	5	2	70
MoS_2/GO	resistive	35−85	∼1700	43	37	71
MoS_2/SiNWA	resistive	11−95	2967	22.2	11.5	26
Pt/MoS_2	resistive	35−85	4000	91.2	153.6	72
2D MoS_2	resistive	0−80	6800	0.6	0.3	73
TiO_2 nanoflowers	resistive	20−95	4.61×10^4	4	<1	74
N-doped TiO_2	resistive	0−90	3.28×10^5	18	299	75
MoS_2-flakes	resistive	10−95	5.3×10^6	8	22	this work

intermediate between the near-unity values of quantum-dot-type nanoparticles[44] and the values typically larger than 10 of nanoflake-type nanoparticles.[45−47] Previous investigations on films of quantum-dot-type MoS_2 nanoparticles have also reported humidity-dependent conductivities.[44] Therefore, we can consider the possibility that small aspect ratio values can be relevant to humidity sensing characteristics.

Humidity-Sensing Results of the MoS_2 film. To probe the sensor's performance, we have carried out dynamic measurements, where the relative humidity is varied continuously. The sensor response was recorded as a function of time with a relative humidity variation of 10−95%. Figure 3a depicts the sensor conductance variation for a fixed applied voltage (+10 V) as a function of RH. Such high voltage is needed because of the high resistance of MoS_2 films. One can note that the conductance changes by 6 orders of magnitude between 10−95% of RH. Results for different devices can be found in the Supporting Information. The sensitivity (S) of the MoS_2 humidity sensor can be defined as[48]

$$S = [(I_{RH} - I_{10})/I_{10}] \times 100\% \quad (1)$$

where I_{RH} and I_{10} represent the device's current values at the humidity atmosphere and at 10% RH, respectively. The inset of Figure 3a shows the device sensitivity S in log scale versus RH, for RH between 10 and 95%. A detailed view of S in the range of 10−20% is shown in Figure S5 of the Supporting Information file. The sensitivity reaches a maximum value of 10^6%. The sensitivity results for different devices can be found in Figure S6 of the Supporting Information file.

Table 1 displays a comparison between the type of electrical response monitored (impedance, capacitive, and resistive) for different RH sensor materials reported in the literature, along with their sensitivity, recovery, and response time. Several materials have been used for humidity sensors in composite or in a single phase, having different properties like high thermal conductivity, high electrical conductivity, and good chemical and mechanical stabilities. Our sensor sensitivity is one of the highest achieved for resistive-type sensors and comparable with those obtained by other measurement techniques.

The repeatability of the MoS_2 ink sensor was assessed via consecutive tests of adsorption and desorption processes, switching the RH level for 10 cycles between ∼20% RH (for 4 min) and 50% RH (for 1.5 min); see Figure 3b. In the adsorption (desorption) process, the sensor's current increases (decreases) with the increase (decrease) of the relative humidity. As shown in Figure 3b, the current variation was almost identical for all cycles performed for more than 50 min indicating excellent repeatability. Next, the sensor stability was studied for several consecutive days, evaluating the sensitivity at 50 and 90% relative humidity, as shown in Figure 3c. The current variation was less than 10% for each humidity region probed. The device also shows a very stable response with minimal performance fluctuation after 35 days, demonstrating critical long-term stability.

https://doi.org/10.1021/acsomega.1c06525
ACS Omega 2022, 7, 9388−9396

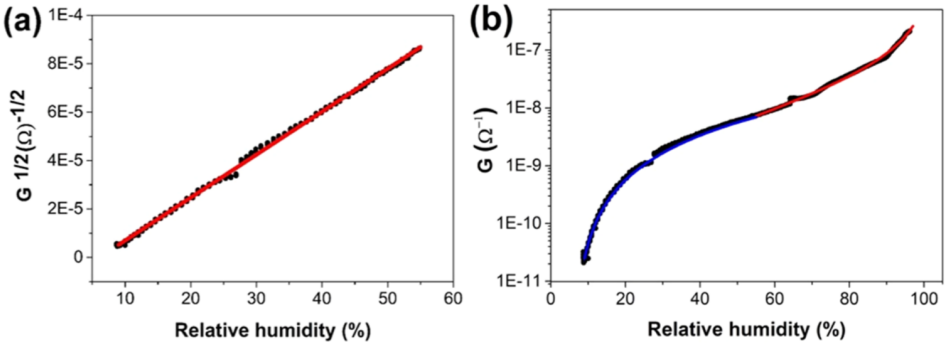

Figure 4. (a) Square root of the conductance, $\sqrt{G}$, versus RH for humidity values below 55%. (b) Fitting of the conductance G as a function of relative humidity with eq 4 (in blue) and (5) (in red).

Figure 3d compares the current response of the MoS_2 sensor with a commercial capacitive humidity sensor model AM2303 DHT22 response, both normalized. The MoS_2 sensor variation between the two states is fast, stable, and reversible. Figure 3d shows that the MoS_2 sensor response time (to a suddenly increased humidity) is similar to that of the commercial sensor, but it also shows that the MoS_2 sensor recovery time (to a suddenly reduced humidity) is faster than that of the commercial sensor investigated. The response time relative to an RH increase from 85 to 87% is 8 s. Conversely, the recovery time to an RH decrease from 87 to 85% is 22 s. The difference between the response and recovery times can be ascribed to the higher humidity sensitivity response and higher bonding energy between the adsorbed water molecules and the surface of the sensor material.[76,77] Also, Table 1 shows that recovery and response times of our sensor are comparable to most of the humidity sensors reported. Response and recovery times for a wider range variation of humidity can be found in the Supporting Information.

Humidity-Sensing Mechanisms. We will now address possible mechanisms behind the change of conductivity of the MoS_2 film upon interaction with water molecules. Previous studies have investigated this interaction for MoS_2-based composites and exfoliated MoS_2 flakes. The issue is controversial since some works report that H_2O adsorption on MoS_2 results in a decrease of conductivity.[15,49,78] An electron charge transfer process from MoS_2 to water molecules was predicted via density functional theory calculations[79] and also observed in few-layer MoS_2 transistors.[80] On the other hand, other works report an increase of MoS_2 conductivity due to water interaction.[21,26,61,65,71] For instance, conductivity increase with humidity was observed for MoS_2/GO,[71] MoS_2/nanodiamond composites,[61] MoS_2/Si nanowires,[26] and dendritic MoS_2.[21]

In the following, we will consider two analytical models[81,82] that can describe the dependence of the conductivity σ (and, consequently, of the conductance $G = 1/R$) on the relative humidity, in limits of low and high relative humidity (<55 and >55%, respectively). Figure 4a shows $\sqrt{G}$ versus RH for the sensor at the low RH regime. Up to a given value of RH, there is no measurable current through the device. Above a threshold value RH_0, a linear behavior of $\sqrt{G}$ versus RH−RH_0 is shown. By extrapolating such linear behavior down to $G = 0$ (a value that is not experimentally accessible due to maximum resistivity limitations), we obtain an estimation of RH_0 = 6.07%.

The observed linear behavior of $\sqrt{G}$ implies a power-law behavior of σ above the conduction threshold,

$$\sigma = a(\mathrm{RH} - \mathrm{RH}_0)^t \tag{2}$$

with an exponent $t = 2$. As the amount of adsorbed water n has been predicted and observed[83] to increase continuously with RH, we conclude that a power law with the same exponent will occur as a function of n,

$$\sigma = b(n - n_0)^t \tag{3}$$

Now, let us consider that a contiguous adsorbed water layer is the only medium, where conduction can occur, without the possibility of either tunneling or thermal-induced crossing of charge carriers through "dry" regions. Then, the physical situation can be described by standard percolation conductivity,[84] where the conductivity, as a function of n, is predicted to be null up to a critical density n_0, and, at the threshold for conduction, to behave exactly as in eq 3, with universal exponents that only depend on the dimensionality of the network of conducting channels. These exponents can be calculated numerically, leading to values such as $t = 1.310 \pm 0.001$ in two dimensions[85] and $t = 1.998 \pm 0.004$ in three dimensions.[86,87] Therefore, if standard percolation describes the conduction in our devices, the observed exponent $t = 2$ would indicate that the MoS_2 film behaves as a "sponge" of finite thickness, where the adsorbed water can infiltrate and form a 3D network of water channels: a simple 2D water adsorption at the surface would lead to a smaller exponent. Interestingly, Figure 4a also shows that the approximately linear behavior of $\sqrt{\sigma}$ versus RH extends for a wide range of relative humidity, well beyond the humidity RH_0 at the conduction threshold up to about RH ≅ 55%. This provides us a very simple fitting formula for RH < 55%,

$$\sigma = \begin{cases} 0, & \mathrm{RH} < \mathrm{RH}_0 \\ a(\mathrm{RH} - \mathrm{RH}_0)^2, & \mathrm{RH}_0 < \mathrm{RH} < 55\% \end{cases} \tag{4}$$

For values of RH larger than 55%, we will consider that the MoS_2 layer is fully wet and that a contiguous liquid water layer is formed atop it. In this regime, the humidity-induced variation in the electrical transport is associated with changes in the ionic conductivity of the water layer. Such ionic transport is usually ascribed to the Grotthuss mechanism,[81,82] where H_3O^+ ions act as charge carriers in proton-exchange reactions, $H_3O^+ + H_2O \rightarrow H_2O + H_3O^+$. Skinner et al. have proposed an analytical description of the ionic conductivity of a humidity-induced water layer atop an otherwise insulating

https://doi.org/10.1021/acsomega.1c06525
ACS Omega 2022, 7, 9388−9396

solid surface.[88] Their calculations are based on the thermodynamic equilibrium between the water layer and the water vapor, as well as on the thermodynamic equilibrium between unbound (free) ionic carriers in the water layer and corresponding bound ions at the insulating surface. One of their main results is that the 2D density of free carriers n, in the limit of $n \ll n_b$, where n_b is the 2D density of ion binding sites at the surface, is given by $n = \sqrt{n_b}\, n_{H_2O}^{1/3}\, e^{-(-\gamma+\ln\kappa)l_B/d}$, where n_{H_2O} is the 3D density of water molecules in the liquid phase, γ is the Euler constant, κ is the water permittivity, l_B is the Bjerrum length, and d is the thickness of the water layer.[88] Based on that result, Skinner et al. obtained a simple fitting function for the ionic conductivity σ as a function of the relative humidity RH (as shown in Figure 4b),

$$\ln \sigma = \alpha - \beta \ln(100/\mathrm{RH})^{1/3} \quad (5)$$

CONCLUSIONS

In conclusion, we have investigated the humidity-sensing properties of the resistive-type humidity sensor based on MoS_2 ink, which is produced via sonication-based exfoliation. The conductance readout of the sensor can increase up to 6 orders of magnitude upon relative humidity increase from 10 to 95% at room temperature. The MoS_2 ink sensor showed very high sensitivity, excellent stability, repeatability, and good response and recovery times. The humidity-sensing mechanisms of MoS_2 were also discussed in detail. The results showed ideal characteristics for the development of high-performance humidity sensors for real-life applications.

EXPERIMENTAL SECTION

Material Preparation and Fabrication of Humidity Sensor. Molybdenum disulfide ink was prepared by sonication-assisted exfoliation. Briefly, 400 mg of MoS_2 powder (<2 mm, 99%, Aldrich) was dispersed in 250 mL of a 7:3 volume of deionized water and isopropyl alcohol. The exfoliation of MoS_2 in suspension was performed using an ultrasonic probe processer for 3 hours (Sonics Vibra-Cell VCX 2500). After sonication, the dispersion was centrifuged at 2500 rpm for 20 minutes to remove the residue/precipitate, and the yellowish-green supernatant containing the nanoflakes was collected, as described by Coleman and collaborators.[38] This supernatant was stable for six months. The UV−visible spectra of exfoliated MoS_2 are shown in the Support Information. The MoS_2 sensor film was deposited using an aerosol deposition method employing a 0.2 mm airbrush pen (Importway). Briefly, 20 mL of MoS_2 ink was uniformly sprayed by the airbrush in an area of 50 × 4 mm^2 in a copper-clad phenolic sheet or using a PET flexible substrate containing Au/Cr interdigital electrodes (IDEs) previously deposited. During the spraying process, the substrates were kept at 80 °C for rapid evaporation of water from the ink.

Material Characterization and Testing System of Humidity Sensors. The surface morphology of MoS_2 ink films was observed by scanning electron microscopy (SEM, FEI Quanta 200 FEG). The microstructure was characterized by Raman spectroscopy (Witec Alpha300 spectrometer). Atomic force microscopy characterization was carried out on a Bruker MultiMode 8 SPM using the intermittent contact mode and Si cantilevers (DPE/XSC11 hard) from Mikromasch, with spring constants of 7−42 Nm^{-1} and a tip radius of curvature of ∼10 nm. A home-built controlled environmental chamber was used to record the sensor's electrical response upon changes in relative humidity. The humidity level inside the chamber was regulated using electronic mass flow controllers. Water vapor from a bubbler under heating was added to an argon stream to set the chamber's humidity, whereas the second stream of argon was used for dehumidification and for purging. A commercial temperature and humidity sensor (AM2302 DHT22, precision of 2% RH), based on a capacitor with a hygroscopic polymer as dielectric, was used as a reference and feedback. The commercial sensor and the MoS_2 film sensor responses were continuously monitored. The temperature for the whole experiment was maintained at 25 °C. In addition, the bubbler's heating temperature was also controlled to keep the humidity approximately constant or to obtain different values of relative humidity inside the chamber. Figure S3 of the Supporting Information shows a detailed schematic of the characterization setup.

ASSOCIATED CONTENT

Supporting Information

The Supporting Information is available free of charge at https://pubs.acs.org/doi/10.1021/acsomega.1c06525.

Characterization of MoS_2 ink by UV−vis; preparation of copper-plated phenolites and Au/Cr interdigital electrodes (IDEs); influence of time of the exfoliation on the lateral size by DLS; characterization of the devices with MoS_2 ink; test of MoS_2 ink on the flexible PET substrate; response and recovery times for a large switching of the humidity levels (PDF)

AUTHOR INFORMATION

Corresponding Author

Rodrigo G. Lacerda − *Departamento de Física, Universidade Federal de Minas Gerais, Belo Horizonte, Minas Gerais 31270-90, Brazil; Centro de Tecnologia em Nanomateriais e Grafeno/UFMG, Universidade Federal de Minas Gerais, BHtec, Belo Horizonte, Minas Gerais 31310-260, Brazil;* orcid.org/0000-0003-4777-7370; Email: rlacerda@fisica.ufmg.br

Authors

Neuma M. Pereira − *Departamento de Física, Universidade Federal de Minas Gerais, Belo Horizonte, Minas Gerais 31270-90, Brazil; Departamento de Química, Universidade Federal de Minas Gerais, Belo Horizonte, Minas Gerais 31270-90, Brazil; Centro de Tecnologia em Nanomateriais e Grafeno/UFMG, Universidade Federal de Minas Gerais, BHtec, Belo Horizonte, Minas Gerais 31310-260, Brazil*

Natália P. Rezende − *Departamento de Física, Universidade Federal de Minas Gerais, Belo Horizonte, Minas Gerais 31270-90, Brazil; Centro de Tecnologia em Nanomateriais e Grafeno/UFMG, Universidade Federal de Minas Gerais, BHtec, Belo Horizonte, Minas Gerais 31310-260, Brazil*

Thiago H. R. Cunha − *Departamento de Física, Universidade Federal de Minas Gerais, Belo Horizonte, Minas Gerais 31270-90, Brazil; Centro de Tecnologia em Nanomateriais e Grafeno/UFMG, Universidade Federal de Minas Gerais, BHtec, Belo Horizonte, Minas Gerais 31310-260, Brazil*

https://doi.org/10.1021/acsomega.1c06525
ACS Omega 2022, 7, 9388−9396

Ana P. M. Barboza − *Departamento de Física, Universidade Federal de Ouro Preto, Ouro Preto, Minas Gerais 35400-000, Brazil*

Glaura G. Silva − *Departamento de Química, Universidade Federal de Minas Gerais, Belo Horizonte, Minas Gerais 31270-90, Brazil; Centro de Tecnologia em Nanomateriais e Grafeno/UFMG, Universidade Federal de Minas Gerais, BHtec, Belo Horizonte, Minas Gerais 31310-260, Brazil*

Daniel Lippross − *Departamento de Química, Universidade Federal de Minas Gerais, Belo Horizonte, Minas Gerais 31270-90, Brazil*

Bernardo R. A. Neves − *Departamento de Física, Universidade Federal de Minas Gerais, Belo Horizonte, Minas Gerais 31270-90, Brazil;* orcid.org/0000-0003-0464-4754

Hélio Chacham − *Departamento de Física, Universidade Federal de Minas Gerais, Belo Horizonte, Minas Gerais 31270-90, Brazil;* orcid.org/0000-0001-5041-9094

Andre S. Ferlauto − *Centro de Engenharia, Modelagem e Ciências Sociais Aplicadas, Universidade Federal do ABC, Santo André, São Paulo 09210-580, Brazil; Centro de Tecnologia em Nanomateriais e Grafeno/UFMG, Universidade Federal de Minas Gerais, BHtec, Belo Horizonte, Minas Gerais 31310-260, Brazil;* orcid.org/0000-0003-3056-7289

Complete contact information is available at: https://pubs.acs.org/10.1021/acsomega.1c06525

Notes

The authors declare no competing financial interest.

■ ACKNOWLEDGMENTS

The authors would like to thank Fapemig (Rede 2D and individual projects), INCT Nanomateriais de Carbono, CNPq /MCT, Petrobras, BNDES, and CAPES for the funding support. The authors are also thankful to LabNano, Laboratório de Cristalografia (LabCri), Centro de Microscopia-UFMG, and SISNANO/LCPNano at UFMG.

■ REFERENCES

(1) Wiklund, J.; Karakoç, A.; Palko, T.; Yiğitler, H.; Ruttik, K.; Jäntti, R.; Paltakari, J. A Review on Printed Electronics: Fabrication Methods, Inks, Substrates, Applications and Environmental Impacts. *J. Manuf. Mater. Process.* **2021**, *5*, 89.

(2) Akinwande, D. Two-Dimensional Materials: Printing Functional Atomic Layers. *Nat. Nanotechnol.* **2017**, *12*, 287−288.

(3) Akinwande, D.; Petrone, N.; Hone, J. Two-Dimensional Flexible Nanoelectronics. *Nat. Commun.* **2014**, *5*, No. 5678.

(4) Lima, A. C.; Pereira, N.; Policia, R.; Ribeiro, C.; Correia, V.; Lrerreanceros-Mendez, S.; Martins, P. All-Printed Multilayer Materials with Improved Magnetoelectric Response. *J. Mater. Chem. C* **2019**, *7*, 5394−5400.

(5) Oliveira, J.; Correia, V.; Castro, H.; Martins, P.; Lanceros-Mendez, S. Polymer-Based Smart Materials by Printing Technologies: Improving Application and Integration. *Addit. Manuf.* **2018**, *21*, 269−283.

(6) Hu, Y.; Zhao, T.; Zhu, P.; Zhu, Y.; Shuai, X.; Liang, X.; Sun, R.; Lu, D. D.; Wong, C.-P. Low Cost and Highly Conductive Elastic Composites for Flexible and Printable Electronics. *J. Mater. Chem. C* **2016**, *4*, 5839−5848.

(7) Chen, Z.; Lu, C. Humidity Sensors: A Review of Materials and Mechanisms. *Sens. Lett.* **2005**, *3*, 274−295.

(8) Hashim, A.; Al-Khafaji, Y.; Hadi, A. Synthesis and Characterization of Flexible Resistive Humidity Sensors Based on PVA/PEO/CuO Nanocomposites. *Trans. Electr. Electron. Mater.* **2019**, *20*, 530−536.

(9) Alrammouz, R.; Podlecki, J.; Vena, A.; Garcia, R.; Abboud, P.; Habchi, R.; Sorli, B. Highly Porous and Flexible Capacitive Humidity Sensor Based on Self-Assembled Graphene Oxide Sheets on a Paper Substrate. *Sens. Actuators, B* **2019**, *298*, No. 126892.

(10) Kim, H.; Park, S.; Park, Y.; Choi, D.; Yoo, B.; Lee, C. S. Fabrication of a Semi-Transparent Flexible Humidity Sensor Using Kinetically Sprayed Cupric Oxide Film. *Sens. Actuators, B* **2018**, *274*, 331−337.

(11) Mattana, G.; Kinkeldei, T.; Leuenberger, D.; Ataman, C.; Ruan, J.; Molina-Lopez, F.; Vásquez Quintero, A.; Nisato, G.; Troster, G.; Briand, D.; Rooij, N. Woven Temperature and Humidity Sensors on Flexible Plastic Substrates for E-Textile Applications. *Sensors Journal, IEEE* **2013**, *13*, 3901−3909.

(12) Yang, T.; Yu, Y. Z.; Zhu, L. S.; Wu, X.; Wang, X. H.; Zhang, J. Fabrication of Silver Interdigitated Electrodes on Polyimide Films via Surface Modification and Ion-Exchange Technique and Its Flexible Humidity Sensor Application. *Sens. Actuators, B* **2015**, *208*, 327−333.

(13) Balde, M.; Vena, A.; Sorli, B. Fabrication of Porous Anodic Aluminium Oxide Layers on Paper for Humidity Sensors. *Sens. Actuators, B* **2015**, *220*, 829−839.

(14) Zhang, D.; Zong, X.; Wu, Z.; Zhang, Y. Hierarchical Self-Assembled SnS2 Nanoflower/Zn2SnO4 Hollow Sphere Nanohybrid for Humidity-Sensing Applications. *ACS Appl. Mater. Interfaces* **2018**, *10*, 32631−32639.

(15) Park, S. Y.; Lee, J. E.; Kim, Y. H.; Kim, J. J.; Shim, Y. S.; Kim, S. Y.; Lee, M. H.; Jang, H. W. Room Temperature Humidity Sensors Based on RGO/MoS2 Hybrid Composites Synthesized by Hydrothermal Method. *Sens. Actuators, B* **2018**, *258*, 775−782.

(16) Rahim, I.; Shah, M.; Khan, A.; Luo, J.; Zhong, A.; Li, M.; Ahmed, R.; Li, H.; Wei, Q.; Fu, Y. Capacitive and Resistive Response of Humidity Sensors Based on Graphene Decorated by PMMA and Silver Nanoparticles. *Sens. Actuators, B* **2018**, *267*, 42−50.

(17) Courbat, J.; Kim, Y. B.; Briand, D.; Rooij, N. F. de. Inkjet Printing on Paper for the Realization of Humidity and Temperature Sensors. In *2011 16th International Solid-State Sensors, Actuators and Microsystems Conference*; **2011**; 1356−1359.

(18) Kafy, A.; Akther, A.; Shishir, M. I. R.; Kim, H. C.; Yun, Y.; Kim, J. Cellulose Nanocrystal/Graphene Oxide Composite Film as Humidity Sensor. *Sens. Actuators, A* **2016**, *247*, 221−226.

(19) Zhang, D.; Wang, M.; Zhang, W.; Li, Q. Flexible Humidity Sensing and Portable Applications Based on MoSe2 Nanoflowers/Copper Tungstate Nanoparticles. *Sens. Actuators, B* **2020**, *304*, No. 127234.

(20) Burman, D.; Choudhary, D. S.; Guha, P. K. ZnO/MoS2-Based Enhanced Humidity Sensor Prototype With Android App Interface for Mobile Platform. *IEEE Sens. J.* **2019**, *19*, 3993−3999.

(21) Ren, J.; Guo, B.; Feng, Y.; Yu, K. Few-Layer MoS2 Dendrites as a Highly Active Humidity Sensor. *Phys. E* **2020**, *116*, No. 113782.

(22) Novoselov, K. S.; Jiang, D.; Schedin, F.; Booth, T. J.; Khotkevich, V. V.; Morozov, S. V.; Geim, A. K. Two-Dimensional Atomic Crystals. *Proc. Natl. Acad. Sci. U.S.A.* **2005**, *102*, 10451−10453.

(23) Worsley, R.; Pimpolari, L.; McManus, D.; Ge, N.; Ionescu, R.; Wittkopf, J. A.; Alieva, A.; Basso, G.; Macucci, M.; Iannaccone, G.; Novoselov, K. S.; Holder, H.; Fiori, G.; Casiraghi, C. All-2D Material Inkjet-Printed Capacitors: Toward Fully Printed Integrated Circuits. *ACS Nano* **2019**, *13*, 54−60.

(24) Donarelli, M.; Prezioso, S.; Perrozzi, F.; Bisti, F.; Nardone, M.; Giancaterini, L.; Cantalini, C.; Ottaviano, L. Response to NO2 and Other Gases of Resistive Chemically Exfoliated MoS2-Based Gas Sensors. *Sens. Actuators, B* **2015**, *207*, 602−613.

(25) Rezende, N. P.; Cadore, A. R.; Gadelha, A. C.; Pereira, C. L.; Ornelas, V.; Watanabe, K.; Taniguchi, T.; Ferlauto, A. S.; Malachias, A.; Campos, L. C.; Lacerda, R. G. Probing the Electronic Properties of Monolayer MoS2 via Interaction with Molecular Hydrogen. *Adv. Electron. Mater.* **2019**, *5*, No. 1800591.

(26) Lou, Z.; Wu, D.; Bu, K.; Xu, T.; Shi, Z.; Xu, J.; Tian, Y.; Li, X. Dual-Mode High-Sensitivity Humidity Sensor Based on MoS2/Si Nanowires Array Heterojunction. *J. Alloys Compd.* **2017**, *726*, 632−637.
(27) Torrisi, F.; Hasan, T.; Wu, W.; Sun, Z.; Lombardo, A.; Kulmala, T. S.; Hsieh, G.-W.; Jung, S.; Bonaccorso, F.; Paul, P. J.; Chu, D.; Ferrari, A. C. Inkjet-Printed Graphene Electronics. *ACS Nano* **2012**, *6*, 2992−3006.
(28) Zheng, J.; Zhang, H.; Dong, S.; Liu, Y.; Tai Nai, C.; Suk Shin, H.; Young Jeong, H.; Liu, B.; Ping Loh, K. High Yield Exfoliation of Two-Dimensional Chalcogenides Using Sodium Naphthalenide. *Nat. Commun.* **2014**, *5*, No. 2995.
(29) Li, J.; Naiini, M.; Vaziri, S.; Lemme, M.; Östling, M. Inkjet Printing of MoS2. *Adv. Funct. Mater.* **2014**, *24*, 6524−6531.
(30) Finn, D. J.; Lotya, M.; Cunningham, G.; Smith, R. J.; McCloskey, D.; Donegan, J. F.; Coleman, J. N. Inkjet Deposition of Liquid-Exfoliated Graphene and MoS2 Nanosheets for Printed Device Applications. *J. Mater. Chem. C* **2014**, *2*, 925−932.
(31) Forsberg, V.; Zhang, R.; Andersson, H.; Bäckström, J.; Dahlström, C.; Norgren, M.; Andres, B.; Olin, H. Liquid Exfoliation of Layered Materials in Water for Inkjet Printing. *J. Imaging Sci. Technol.* **2016**, *60*, No. 040405.
(32) Paolucci, V.; D'Olimpio, G.; Lozzi, L.; Mio, A. M.; Ottaviano, L.; Nardone, M.; Nicotra, G.; Le-Cornec, P.; Cantalini, C.; Politano, A. Sustainable Liquid-Phase Exfoliation of Layered Materials with Nontoxic Polarclean Solvent. *ACS Sustain. Chem. Eng.* **2020**, *8*, 18830−18840.
(33) Orrill, M.; Abele, D.; Wagner, M.; LeBlanc, S. Ink Synthesis and Inkjet Printing of Electrostatically Stabilized Multilayer Graphene Nanoshells. *J. Colloid Interface Sci.* **2020**, *566*, 454−462.
(34) McManus, D.; Vranic, S.; Withers, F.; Sanchez-Romaguera, V.; Macucci, M.; Yang, H.; Sorrentino, R.; Parvez, K.; Son, S.-K.; Iannaccone, G.; Kostarelos, K.; Fiori, G.; Casiraghi, C. Water-Based and Biocompatible 2D Crystal Inks for All-Inkjet-Printed Heterostructures. *Nat. Nanotechnol.* **2017**, *12*, 343.
(35) McManus, D.; Dal Santo, A.; Selvasundaram, P. B.; Krupke, R.; LiBassi, A.; Casiraghi, C. Photocurrent Study of All-Printed Photodetectors on Paper Made of Different Transition Metal Dichalcogenide Nanosheets. *Flex. Print. Electron.* **2018**, *3*, No. 34005.
(36) Casiraghi, C.; Macucci, M.; Parvez, K.; Worsley, R.; Shin, Y.; Bronte, F.; Borri, C.; Paggi, M.; Fiori, G. Inkjet Printed 2D-Crystal Based Strain Gauges on Paper. *Carbon* **2018**, *129*, 462−467.
(37) Li, D.; Lai, W.-Y.; Zhang, Y.-Z.; Huang, W. Printable Transparent Conductive Films for Flexible Electronics. *Adv. Mater.* **2018**, *30*, No. 1704738.
(38) Coleman, J. N.; Lotya, M.; O'Neill, A.; Bergin, S. D.; King, P. J.; Khan, U.; Young, K.; Gaucher, A.; De, S.; Smith, R. J.; Shvets, I. V.; Arora, S. K.; Stanton, G.; Kim, H.-Y.; Lee, K.; Kim, G. T.; Duesberg, G. S.; Hallam, T.; Boland, J. J.; Wang, J. J.; Donegan, J. F.; Grunlan, J. C.; Moriarty, G.; Shmeliov, A.; Nicholls, R. J.; Perkins, J. M.; Grieveson, E. M.; Theuwissen, K.; McComb, D. W.; Nellist, P. D.; Nicolosi, V. Two-Dimensional Nanosheets Produced by Liquid Exfoliation of Layered Materials. *Science* **2011**, *331*, 568−571.
(39) Lee, C.; Yan, H.; Brus, L. E.; Heinz, T. F.; Hone, J.; Ryu, S. Anomalous Lattice Vibrations of Single- and Few-Layer MoS2. *ACS Nano* **2010**, *4*, 2695−2700.
(40) Li, H.; Zhang, Q.; Yap, C. C. R.; Tay, B. K.; Edwin, T. H. T.; Olivier, A.; Baillargeat, D. From Bulk to Monolayer MoS2: Evolution of Raman Scattering. *Adv. Funct. Mater.* **2012**, *22*, 1385−1390.
(41) Chen, L.; Xue, F.; Li, X.; Huang, X.; Wang, L.; Kou, J.; Wang, Z. L. Strain-Gated Field Effect Transistor of a MoS2−ZnO 2D−1D Hybrid Structure. *ACS Nano* **2016**, *10*, 1546−1551.
(42) Zhang, X.; Qiao, X.-F.; Shi, W.; Wu, J.-B.; Jiang, D.-S.; Tan, P.-H. Phonon and Raman Scattering of Two-Dimensional Transition Metal Dichalcogenides from Monolayer, Multilayer to Bulk Material. *Chem. Soc. Rev.* **2015**, *44*, 2757−2785.
(43) Fernandes, T. F. D.; Miquita, D. R.; Soares, E. M.; Santos, A. P.; Cançado, L. G.; Neves, B. R. A. A Semi-Automated General Statistical Treatment of Graphene Systems. *2D Mater.* **2020**, *7*, No. 025045.
(44) Yadav, S.; Chaudhary, P.; Uttam, K. N.; Varma, A.; Vashistha, M.; Yadav, B. C. Facile Synthesis of Molybdenum Disulfide (MoS2) Quantum Dots and Its Application in Humidity Sensing. *Nanotechnology* **2019**, *30*, No. 295501.
(45) Chacham, H.; Santos, J. C. C.; Pacheco, F. G.; Silva, D. L.; Martins, R. M.; Del'Boccio, J. P.; Soares, E. M.; Altoé, R.; Furtado, C. A.; Plentz, F.; Neves, B. R. A.; Cançado, L. G. Controlling the Morphology of Nanoflakes Obtained by Liquid-Phase Exfoliation: Implications for the Mass Production of 2D Materials. *ACS Appl. Nano Mater.* **2020**, *3*, 12095−12105.
(46) Santos, J.; Prado, M.; Morais, H.; Sousa, S.; Silva-Pinto, E.; Cançado, L.; Neves, B. Topological Vectors as a Fingerprinting System for 2D-Material Flake Distributions. *npj 2D Mater. Appl.* **2021**, *5*, No. 51.
(47) Backes, C.; Campi, D.; Szydlowska, B. M.; Synnatschke, K.; Ojala, E.; Rashvand, F.; Harvey, A.; Griffin, A.; Sofer, Z.; Marzari, N.; Coleman, J. N.; O'Regan, D. D. Equipartition of Energy Defines the Size−Thickness Relationship in Liquid-Exfoliated Nanosheets. *ACS Nano* **2019**, *13*, 7050−7061.
(48) Liu, Y. J.; Hao, L. Z.; Gao, W.; Liu, Y. M.; Li, G. X.; Xue, Q. Z.; Guo, W. Y.; Yu, L. Q.; Wu, Z. P.; Liu, X. H.; Zeng, H. Z.; Zhu, J. Growth and Humidity-Dependent Electrical Properties of Bulk-like MoS2 Thin Films on Si. *RSC Adv.* **2015**, *5*, 74329−74335.
(49) Zhao, J.; Li, N.; Yu, H.; Wei, Z.; Liao, M.; Chen, P.; Wang, S.; Shi, D.; Sun, Q.; Zhang, G. Highly Sensitive MoS(2) Humidity Sensors Array for Noncontact Sensation. *Adv. Mater.* **2017**, *29*, No. 1702076.
(50) Sheng, L.; Dajing, C.; Yuquan, C. A Surface Acoustic Wave Humidity Sensor with High Sensitivity Based on Electrospun MWCNT/Nafion Nanofiber Films. *Nanotechnology* **2011**, *22*, No. 265504.
(51) Hassan, G.; Bae, J.; Lee, C. H.; Hassan, A. Wide Range and Stable Ink-Jet Printed Humidity Sensor Based on Graphene and Zinc Oxide Nanocomposite. *J. Mater. Sci. Mater. Electron.* **2018**, *29*, 5806−5813.
(52) Guan, X.; Hou, Z.; Wu, K.; Zhao, H.; Liu, S.; Fei, T.; Zhang, T. Flexible Humidity Sensor Based on Modified Cellulose Paper. *Sens. Actuators, B* **2021**, *339*, No. 129879.
(53) Sajid, M.; Kim, H. B.; Lim, J. H.; Choi, K. H. Liquid-Assisted Exfoliation of 2D HBN Flakes and Their Dispersion in PEO to Fabricate Highly Specific and Stable Linear Humidity Sensors. *J. Mater. Chem. C* **2018**, *6*, 1421−1432.
(54) Siddiqui, G. U.; Sajid, M.; Ali, J.; Kim, S. W.; Doh, Y. H.; Choi, K. H. Wide Range Highly Sensitive Relative Humidity Sensor Based on Series Combination of MoS2 and PEDOT:PSS Sensors Array. *Sens. Actuators, B* **2018**, *266*, 354−363.
(55) Hassan, G.; Sajid, M.; Choi, C. Highly Sensitive and Full Range Detectable Humidity Sensor Using PEDOT:PSS, Methyl Red and Graphene Oxide Materials. *Sci. Rep.* **2019**, *9*, No. 15227.
(56) Duan, Z.; Zhao, Q.; Wang, S.; Huang, Q.; Yuan, Z.; Zhang, Y.; Jiang, Y.; Tai, H. Halloysite Nanotubes: Natural, Environmental-Friendly and Low-Cost Nanomaterials for High-Performance Humidity Sensor. *Sens. Actuators, B* **2020**, *317*, No. 128204.
(57) Si, R.; Xie, X.; Li, T.; Zheng, J.; Cheng, C.; Huang, S.; Wang, C. TiO2/(K,Na)NbO3 Nanocomposite for Boosting Humidity-Sensing Performances. *ACS Sens.* **2020**, *5*, 1345−1353.
(58) Sajid, M.; Kim, H. B.; Yang, Y. J.; Jo, J.; Choi, K. H. Highly Sensitive BEHP-Co-MEH:PPV + Poly(Acrylic Acid) Partial Sodium Salt Based Relative Humidity Sensor. *Sens. Actuators, B* **2017**, *246*, 809−818.
(59) Komazaki, Y.; Uemura, S. Stretchable, Printable, and Tunable PDMS-CaCl2 Microcomposite for Capacitive Humidity Sensors on Textiles. *Sens. Actuators, B* **2019**, *297*, No. 126711.
(60) McGhee, J. R.; Sagu, J. S.; Southee, D. J.; Evans, P. S. A.; Wijayantha, K. G. U. Printed, Fully Metal Oxide, Capacitive Humidity Sensors Using Conductive Indium Tin Oxide Inks. *ACS Appl. Electron. Mater.* **2020**, *2*, 3593−3600.

https://doi.org/10.1021/acsomega.1c06525
ACS Omega 2022, 7, 9388−9396

(61) Yu, X.; Chen, X.; Ding, X.; Yu, X.; Zhao, X.; Chen, X. Facile Fabrication of Flower-like MoS2/Nanodiamond Nanocomposite toward High-Performance Humidity Detection. *Sens. Actuators, B* **2020**, *317*, No. 128168.
(62) Rivadeneyra, A.; Salmeron, J. F.; Murru, F.; Lapresta-Fernández, A.; Rodríguez, N.; Capitan-Vallvey, L. F.; Morales, D. P.; Salinas-Castillo, A. Carbon Dots as Sensing Layer for Printed Humidity and Temperature Sensors. *Nanomaterials.* **2020**, *10*, No. 122446.
(63) Li, X.; Chen, X.; Chen, X.; Ding, X.; Zhao, X. High-Sensitive Humidity Sensor Based on Graphene Oxide with Evenly Dispersed Multiwalled Carbon Nanotubes. *Mater. Chem. Phys.* **2018**, *207*, 135−140.
(64) Ahmad, W.; Jabbar, B.; Ahmad, I.; Mohamed Jan, B.; Stylianakis, M. M.; Kenanakis, G.; Ikram, R. Highly Sensitive Humidity Sensors Based on Polyethylene Oxide/CuO/Multi Walled Carbon Nanotubes Composite Nanofibers. *Materials* **2021**, *14*, No. 1037.
(65) Zhang, D.; Sun, Y.; Li, P.; Zhang, Y. Facile Fabrication of MoS2-Modified SnO2 Hybrid Nanocomposite for Ultrasensitive Humidity Sensing. *ACS Appl. Mater. Interfaces* **2016**, *8*, 14142−14149.
(66) Turkani, V. S.; Maddipatla, D.; Narakathu, B. B.; Saeed, T. S.; Obare, S. O.; Bazuin, B. J.; Atashbar, M. Z. A Highly Sensitive Printed Humidity Sensor Based on a Functionalized MWCNT/HEC Composite for Flexible Electronics Application. *Nanoscale Adv.* **2019**, *1*, 2311−2322.
(67) Zhang, D.; Chang, H.; Liu, R. Humidity-Sensing Properties of One-Step Hydrothermally Synthesized Tin Dioxide-Decorated Graphene Nanocomposite on Polyimide Substrate. *J. Electron. Mater.* **2016**, *45*, 4275−4281.
(68) Zhang, R.; Peng, B.; Yuan, Y. Flexible Printed Humidity Sensor Based on Poly(3,4-Ethylenedioxythiophene)/Reduced Graphene Oxide/Au Nanoparticles with High Performance. *Compos. Sci. Technol.* **2018**, *168*, 118−125.
(69) Zhang, X.; Turkani, V. S.; Hajian, S.; Bose, A. K.; Maddipatla, D.; Hanson, A. J.; Narakathu, B. B.; Atashbar, M. Z. In *Novel Printed Carbon Nanotubes Based Resistive Humidity Sensors*, 2019 IEEE International Conference on Flexible and Printable Sensors and Systems (FLEPS), 2019; pp 1−3.
(70) Jin, X.-F.; Liu, C.-R.-L.; Chen, L.; Zhang, Y.; Zhang, X.-J.; Chen, Y.-M.; Chen, J.-J. Inkjet-Printed MoS2/PVP Hybrid Nanocomposite for Enhanced Humidity Sensing. *Sens. Actuators, A* **2020**, *316*, No. 112388.
(71) Burman, D.; Ghosh, R.; Santra, S.; Guha, P. K. Highly Proton Conducting MoS2/Graphene Oxide Nanocomposite Based Chemoresistive Humidity Sensor. *RSC Adv.* **2016**, *6*, 57424−57433.
(72) Burman, D.; Santra, S.; Pramanik, P.; Guha, P. K. Pt Decorated MoS2nanoflakes for Ultrasensitive Resistive Humidity Sensor. *Nanotechnology* **2018**, *29*, No. 115504.
(73) Zeeshan Yousaf, H. M.; Kim, S. W.; Hassan, G.; Karimov, K.; Choi, K. H.; Sajid, M. Highly Sensitive Wide Range Linear Integrated Temperature Compensated Humidity Sensors Fabricated Using Electrohydrodynamic Printing and Electrospray Deposition. *Sens. Actuators, B* **2020**, *308*, No. 127680.
(74) Jeong, H.; Noh, Y.; Lee, D. Highly Stable and Sensitive Resistive Flexible Humidity Sensors by Means of Roll-to-Roll Printed Electrodes and Flower-like TiO2 Nanostructures. *Ceram. Int.* **2019**, *45*, 985−992.
(75) Li, Z.; Haidry, A. A.; Dong, B.; Sun, L.; Fatima, Q.; Xie, L.; Yao, Z. Facile Synthesis of Nitrogen Doped Ordered Mesoporous TiO2 with Improved Humidity Sensing Properties. *J. Alloys Compd.* **2018**, *742*, 814−821.
(76) Zhao, J.; Liu, Y.; Li, X.; Lu, G.; You, L.; Liang, X.; Liu, F.; Zhang, T.; Du, Y. Highly Sensitive Humidity Sensor Based on High Surface Area Mesoporous LaFeO3 Prepared by a Nanocasting Route. *Sens. Actuators, B* **2013**, *181*, 802−809.
(77) Wang, J.-G.; Zhang, L.-X.; Yin, J.; Zhao, L.-X.; Bie, L.-J. Layered K(K1.5Eu0.5)Ta3O10 for Humidity Sensor. *Measurement* **2016**, *82*, 151−154.
(78) Zhang, S. L.; Choi, H. H.; Yue, H. Y.; Yang, W. C. Controlled Exfoliation of Molybdenum Disulfide for Developing Thin Film Humidity Sensor. *Curr. Appl. Phys.* **2014**, *14*, 264−268.
(79) Yue, Q.; Shao, Z.; Chang, S.; Li, J. Adsorption of Gas Molecules on Monolayer MoS2 and Effect of Applied Electric Field. *Nanoscale Res. Lett.* **2013**, *8*, No. 425.
(80) Late, D. J.; Huang, Y.-K.; Liu, B.; Acharya, J.; Shirodkar, S. N.; Luo, J.; Yan, A.; Charles, D.; Waghmare, U. V.; Dravid, V. P.; Rao, C. N. R. Sensing Behavior of Atomically Thin-Layered MoS2 Transistors. *ACS Nano* **2013**, *7*, 4879−4891.
(81) Bi, H.; Yin, K.; Xie, X.; Ji, J.; Wan, S.; Sun, L.; Terrones, M.; Dresselhaus, M. S. Ultrahigh Humidity Sensitivity of Graphene Oxide. *Sci. Rep.* **2013**, *3*, No. 2714.
(82) Agmon, N. CHEMICAL PHYSICS The Grotthuss Mechanism. *Chem. Phys. Lett.* **1995**, *244*, 456−462.
(83) Theillet, P.-O.; Pierron, O. N. Quantifying Adsorbed Water Monolayers on Silicon MEMS Resonators Exposed to Humid Environments. *Sens. Actuators, A* **2011**, *171*, 375−380.
(84) Sahimi, M.; Hughes, B. D.; Scriven, L. E.; Davis, H. T. Critical Exponent of Percolation Conductivity by Finite-Size Scaling. *J. Phys. C: Solid State Phys.* **1983**, *16*, L521−L527.
(85) Grassberger, P. Conductivity Exponent and Backbone Dimension in 2-d Percolation. *Phys. A* **1999**, *262*, 251−263.
(86) Hu, H.; Blöte, H. W. J.; Ziff, R. M.; Deng, Y. Short-Range Correlations in Percolation at Criticality. *Phys. Rev. E* **2014**, *90*, No. 042106.
(87) Kozlov, B.; Laguës, M. Universality of 3D Percolation Exponents and First-Order Corrections to Scaling for Conductivity Exponents. *Phys. A* **2010**, *389*, 5339−5346.
(88) Skinner, B.; Loth, M. S.; Shklovksii, B. I. Ionic Conductivity on a Wetting Surface. *Phys. Rev. E: Stat., Nonlinear, Soft Matter Phys.* **2009**, *80*, No. 041925.

https://doi.org/10.1021/acsomega.1c06525
ACS Omega 2022, 7, 9388−9396